Optics Communications 387 (2017) 141–147

Contents lists available at ScienceDirect

Optics Communications

journal homepage: www.elsevier.com/locate/optcom

Spatial, polarization and angular characteristics of external conical refraction

V.V. Filippov

Belarusian State University of Informatics and Radioelectronics, P. Brovka Str. 6, 220013 Minsk, Belarus

ARTICLE INFO

Keywords:
Biaxial crystals
Optic axes
Conical refraction
Ray cone
Dispersion

ABSTRACT

Appearance of two rings of external conical refraction (ECR) is investigated theoretically within the plane-wave approximation. The hollow cone of ECR is the cone of normals inside a crystal. Due to a birefringence, two sets of isonormal waves are related to the cone. One set forms a filament of rays directed along the biradial, and the other set generates the hollow cone of rays. The apex angle of the cone is nearly twice as large as that of the cone of normals and its axis is close to the direction of the biradial. After leaving the exit facet of a crystal plate, the ray filament spreads into a cone again, and the ray cone gives rise to a second outer cone so that two nonconcentric rings appear at a screen behind the plate. Polarization states at the neighbouring points of the rings lying on one radius are mutually perpendicular. Numerical calculations were performed for crystals with moderate and large optical anisotropy, namely $KGd(WO_4)_2$, ammonium oxalate, L-N-(5-Nitro-2-peridyl) leucinol and sulfur. Dispersion of the angle of ECR, the apex angle of the cone of incident (from air) waves and the ray cone is calculated for three tungstate crystals, $KGd(WO_4)_2$, $KLu(WO_4)_2$, and $KY(WO_4)_2$.

1. Introduction

The phenomenon of external conical refraction (ECR) was predicted simultaneously with internal conical refraction (ICR) by Hamilton in 1832 and their existence shortly after was confirmed experimentally by Lloyd [1]. Since then, a lot of attention has been paid to the investigation of ICR (see, for example, [2], where the main steps in the study of ICR are presented). The essential features of this phenomenon can be described within a simple plane wave approximation [3–5]. Full and detailed picture of conical refraction is deduced using different models of real beams with a finite size [6–9] (the so-called internal "conical diffraction" [10]).

ICR attracts more and more interest during the last years. The renewed interest to the phenomenon is mostly related to demonstration of efficient conical refraction lasers [11,12] with excellent beam quality and its application in optical manipulators [13] and mode convertors [14]. Interesting features were observed when a convergent beam passed through a biaxial crystal along one of its optic axis. Being transformed by ICR, the emerging light pattern showed a complex evolution upon propagation and a very complicated spatial structure [8,15,16]. A good agreement between theoretical description and experimental observations has been demonstrated taking into account the diffraction of electromagnetic wave propagating through a biaxial crystal and interference of light behind the exit face of the crystal. It should be mentioned also the theoretical description and experimental results on ICR in chiral and nonlinear crystals (see [17–22] and references therein).

In contrast to ICR, very few studies of ECR are known to date [23–29]. Meanwhile a possibility to obtain high intensity densities within the crystal due to ECR is an attractive peculiarity of the phenomenon which especially becomes interesting for nonlinear effects like Raman shifting or phase conjugations [27]. The polarization dependence of ECR was demonstrated for ammonium oxalate and lithium formate [23] and, as it was stated in [24], the polarization distribution on the cone of ECR is the same as in the case of ICR. The measured in [24] angle of the cone of the external conical refraction in air for KTN crystal (3°24′) was in accordance with the calculated value (3°13′). In both works only one bright ring related to the ECR cone was observed on a screen behind the crystal. However, later on Mikhailichenko showed the existence of two bright rings [25,26]. The appearance of second ring was explained by influence of the birefringence (it was marked also in [28]). Thus, this situation outwardly reminds finding the double rings for ICR and the subsequent explanation of the phenomenon on the basis of a double refraction of a bounded light beam. Nevertheless, both effects are observed under conditions that are not identical. ICR occurs for a single direction in a crystal (i.e., the wave optical axis) for which the double refraction is absent. Then, when dealing with a bounded divergent light beam, we include the effects of a double refraction into the consideration. On the contrary, ECR phenomenon takes place for a direction with a double refraction (namely, the

E-mail address: filippov@dragon.bas-net.by.

http://dx.doi.org/10.1016/j.optcom.2016.11.050
Received 1 November 2016; Received in revised form 18 November 2016; Accepted 19 November 2016

direction of a ray optical axis). Consideration of bounded light beam propagation in this direction does not change the situation in principle albeit it can bring in new additional details in the phenomenon. In their theoretical study of a bounded (Gaussian) beam propagation along the ray optical axis, Belsky and Khapalyuk marked that, as it can be expected, the structure of the beam after passing a crystal changes insignificantly due to the absence of the wave surface peculiarities for the direction of the ray optical axis [29]. The output beam exhibits astigmatism and elliptical cross-section that is the result of the crystal optical anisotropy. Meanwhile, in the case of ICR, the intensity profile of the output beam in the far-field is asymptotically equal to that of the incident beam [30].

Finally, of special interest are the recent experiments of Cattoor [31]. He showed the possibility of having laser action using the phenomenon of ECR. In his experiments the crystal Ho^{3+}: $KY(WO_4)_2$ was cutted to have ECR for pump beam. This pump scheme allows the divergence of the pump inside the crystal to be reduced. Other peculiarities of the scheme are also noted in [31].

Lloyd in his experiments used a strongly convergent beam incident onto an entrance crystal surface and observed the phenomenon of ECR looking through the aperture. This aperture allowed him to select only those rays from all rays arising in the crystal, direction propagation of which was close to the direction of a biradial. On the other hand, in such experimental scheme it was impossible to observe the second ring of ECR. Quiet different scheme of observation was applied by Mikhailichenko [25,26]. He used a hollow cone of converging waves which was formed by a ring-shaped diaphragm. In such a case there was no need in an exit aperture that allowed him to establish the existence of two rings at a screen behind the crystal plate and to study the polarization distribution along the new ring.

In the present paper, we consider ECR as a double refraction phenomenon for the particular direction (ray optical axis) of wave propagation in a crystal. Parameters of the two cones of ECR which arise in this case and the distribution of the polarization on the cones are calculated analytically and using numerical analysis for different crystals with a moderate (monoclinic double tungstates, MDTs) and large (organic crystals, sulfur) optical anisotropy. MDTs exhibit pronounced nonlinear properties. In particular, they possess large third order nonlinear optical susceptibility that opens possibilities for developing efficient Raman lasers and give rise to other common nonlinear phenomena including two-photon absorption, stimulated Brillouin scattering and self-focusing [32–34]. Considering these possible applications of the phenomenon, dispersion of ECR angles in and out of the crystal is calculated for the three MDTs, namely $KGd(WO_4)_2$, $KLu(WO_4)_2$, and $KY(WO_4)_2$.

2. Basic equations

Both conical refractions (internal and external) can be described from geometrical properties of the characteristic surfaces which are used in crystal-optics. Four conoidal cusps (diabolical points [2]) of an index surface give the optical axes of the crystal or binormals. Internal conical refraction happens when light upon entering a biaxial birefringent crystal along one of the binormals direction, spreads out in it into a hollow cone of rays and exits the crystal slab in the form of a hollow cylinder (two concentric cylinders of light under rigorous examination).

Four conoidal cusps of a wave surface correspond to two optical axes of the second type, ray optical axes or biradials. In the case of external conical refraction a hollow cone of light, converging towards a point on the surface of a biaxial crystal slab, will become (under some conditions) collimated along the optic ray axis of the crystal (if birefringence is not taking into account). When this bundle of rays reaches the opposite facet of the slab, it emerges as an expanding cone of light.

In the wave theory, it is more convenient to relate these phenomena to the properties of a dielectric tensor of the crystal ε which fully describes its wave properties. The tensor has a diagonal form in the right-hand system of the principal axes with the unit vectors $\mathbf{u}_p$, $\mathbf{u}_m$, and $\mathbf{u}_g$ and for biaxial crystals it has three different principal eigenvalues $\varepsilon_i=n_i^2$, where n_j ($j=p, m, g$) are the principal refractive indices of the crystal. Unit vectors (otrs) $\mathbf{u}_p$, $\mathbf{u}_m$, and $\mathbf{u}_g$ coincide with the optical indicatrix axes N_p, N_m, and N_g, respectively. Let us use a dyadic form for the representation of ε. The tensor ε may be written in Fedorov axial dyadic representation [35]:

$$\varepsilon = \varepsilon_p \boldsymbol{u}_p\cdot\boldsymbol{u}_p + \varepsilon_m \boldsymbol{u}_m\cdot\boldsymbol{u}_m + \varepsilon_g \boldsymbol{u}_g\cdot\boldsymbol{u}_g = \varepsilon_m + \frac{\varepsilon_g-\varepsilon_p}{2}(\boldsymbol{c}_1\cdot\boldsymbol{c}_2 + \boldsymbol{c}_1\cdot\boldsymbol{c}_2). \tag{1}$$

Here, the dot indicates a direct product of vectors (diad); in the coordinate representation, $(\boldsymbol{a}\,\boldsymbol{c})_{ik}=a_i c_k$. The convolution of a diad with a vector is a vector and it reduces to a scalar multiplication of two adjacent vectors, for example, $(\boldsymbol{a}\,\boldsymbol{c})\boldsymbol{u}=\boldsymbol{c}\boldsymbol{u}\,\boldsymbol{a}$. The unit vectors $\boldsymbol{c}_1$ and $\boldsymbol{c}_2$ give directions of the two ray optical axes or biradials:

$$\boldsymbol{c}_1 = k_p\boldsymbol{u}_p + k_g\boldsymbol{u}_g, \tag{2a}$$

$$\boldsymbol{c}_2 = -k_p\boldsymbol{u}_p + k_g\boldsymbol{u}_g, \tag{2b}$$

where

$$k_p = \sqrt{\frac{\varepsilon_m-\varepsilon_p}{\varepsilon_g-\varepsilon_p}}, \qquad k_g = \sqrt{\frac{\varepsilon_g-\varepsilon_m}{\varepsilon_g-\varepsilon_p}}. \tag{3}$$

The axial representation of the inverse tensor $\varepsilon^{-1}=(1/\varepsilon_p)\boldsymbol{u}_p\cdot\boldsymbol{u}_p+(1/\varepsilon_m)\,\boldsymbol{u}_m\cdot\boldsymbol{u}_m+(1/\varepsilon_g)\boldsymbol{u}_g\cdot\boldsymbol{u}_g$ determines the optical axes (binormals) of a biaxial crystal:

$$\mathbf{c}_1' = k_p'\mathbf{u}_p + k_g'\mathbf{u}_g, \tag{4a}$$

$$\mathbf{c}_2' = k_p'\mathbf{u}_p - k_g'\mathbf{u}_g, \tag{4b}$$

where

$$k_p' = \frac{\varepsilon_g}{\varepsilon_m}k_p, \quad k_g' = \frac{\varepsilon_p}{\varepsilon_m}k_g. \tag{5}$$

Note that for convenience we marked here the vectors of binormals by prime in contrast to [35,36] where the prime was used for the biradials.

An equation for the cone of ECR follows from the Maxwell's equations and it can be written in the form [36]:

$$\boldsymbol{r}\varepsilon\boldsymbol{r}-\boldsymbol{r}\boldsymbol{c}_1\cdot\boldsymbol{r}\varepsilon\boldsymbol{c}_1 = r_i\varepsilon_{ik}r_k - r_n c_{1n}\cdot r_l\varepsilon_{lm}c_{1m} = 0, \tag{6}$$

where radius-vector $\boldsymbol{r}||\boldsymbol{n}$, $\boldsymbol{n}$ is a wave normal ($\boldsymbol{n}^2=1$). From this equation it follows that $\mathbf{c}_1$ and a vector $\boldsymbol{g}_N$:

$$\boldsymbol{g}_N = \varepsilon^{-1}\mathrm{c}_1 = \frac{1}{\varepsilon_p}k_p\mathrm{u}_p + \frac{1}{\varepsilon_g}k_g\mathrm{u}_g \tag{7}$$

are two the cone generators. To find the cross-section of the cone by a plane located at a distance l from its vertex and perpendicular to the biradial $\boldsymbol{c}_1$ ($\boldsymbol{r}= l\boldsymbol{c}_1+\boldsymbol{r}'$, where $\boldsymbol{r}'\perp\boldsymbol{c}_1$), we introduce a unit vector $\boldsymbol{d}$mutually orthogonal to the vectors $\boldsymbol{u}_\mathrm{m}$ and $\mathbf{c}_1$, so:

$$\boldsymbol{d} = k_g\boldsymbol{u}_p - k_p\boldsymbol{u}_g, \tag{8}$$

and we decompose the plane radius-vector $\boldsymbol{r}'$onto two components:$\boldsymbol{r}'=\boldsymbol{r}'\boldsymbol{d}\cdot\boldsymbol{d}+\boldsymbol{r}'\boldsymbol{u}_m\cdot\boldsymbol{u}_m$. Taking into account that $\boldsymbol{r}'\boldsymbol{c}_1=0$ and according to Eqs. (1) and (8), $\boldsymbol{r}'\varepsilon\boldsymbol{r}'=\varepsilon_m\boldsymbol{r}'^2$ and $\boldsymbol{r}'\varepsilon\boldsymbol{c}_1=(1/2)(\varepsilon_g-\varepsilon_m)\boldsymbol{d}\boldsymbol{c}_2$, where $\boldsymbol{d}\boldsymbol{c}_2=-2k_pk_g$, finally we find:

$$\boldsymbol{r}'^2 - \frac{\varepsilon_g-\varepsilon_p}{\varepsilon_m}lk_pk_g\boldsymbol{r}'\boldsymbol{d} = 0 \;or\; \left(\boldsymbol{r}' - \frac{\varepsilon_g-\varepsilon_p}{2\varepsilon_m}lk_pk_g\boldsymbol{d}\right)^2 = \left(\frac{\varepsilon_g-\varepsilon_p}{2\varepsilon_m}lk_pk_g\right)^2. \tag{9}$$

This is an equation of a circle of radius $R=(1/2)(\varepsilon_g-\varepsilon_m)lk_pk_g$ with a center at $(1/2)(\varepsilon_g-\varepsilon_m)lk_pk_g\boldsymbol{d}$, and so the apex angle of the cone of normals of ECR χ_N is equal to *arctan (2R/l)* or

$$\chi_N = arc\,\tan\frac{\sqrt{(\varepsilon_g-\varepsilon_m)(\varepsilon_m-\varepsilon_p)}}{\varepsilon_m}, \tag{10}$$

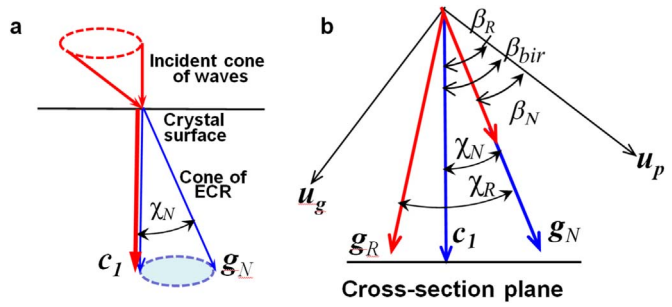

Fig. 1. (a) The cone of ECR inside a crystal as a result of refraction of a hollow cone of incident waves; all rays coincide with $\boldsymbol{c}_1$ (direction of the biradial). (b) Cross-section of the cone of ECR (cone of normals) defined by vectors $\boldsymbol{g}_N$, and $\boldsymbol{c}_1$ and the ray cone defined by vectors $\boldsymbol{g}_N$ and $\boldsymbol{g}_R$.

that coincides with the well-known expression [28]. The cone of ECR arising due to the refraction of a hollow cone of incident waves schematically is shown in Fig. 1(a).

For all wave normals belonging to the cone expressed by Eq. (6), the birefringence should occur. This means that two waves can propagate along any cone generator. Their polarizations are mutually orthogonal, and the refractive indices and the directions of the energy flux (rays) are different. For one of the two waves, the ray is always parallel to the biradial $\boldsymbol{c}_1$ (the phenomenon of ECR), while for the second one, this is not the case. Thus, we should find the cone of rays caused by double refraction of waves with normals located at the cone of external conical refraction, see Eq. (6). It is worth, however, to start with a special case of the principal plane of the optical indicatrix orthogonal to the N_m principal axis (or to the ort $\boldsymbol{u}_m$). This plane contains all optical axes of a crystal and the cone generators $\boldsymbol{g}_N$ and $\boldsymbol{c}_1$. One of the isonormal waves with a vector $\boldsymbol{E}$ (and an electrical induction $\boldsymbol{D}$) polarized perpendicular to the plane propagates in this plane as an ordinary (o) wave in the uniaxial crystals, i.e., its refractive index ($n_o=\varepsilon_m^{1/2}$) does not depend on the propagation direction and its ray vector $\boldsymbol{p}_o$ is parallel to $\boldsymbol{n}$. The behavior of the second wave with a vector $\boldsymbol{D}$ located in the plane is similar to the behavior of an extraordinary (e) wave in uniaxial crystals. So, we have [35,36]:

$$\boldsymbol{p}_o = \frac{\boldsymbol{n}}{\varepsilon_m}, \qquad \boldsymbol{p}_e = n_e\frac{\varepsilon\boldsymbol{n}}{\varepsilon_p\varepsilon_g}, \qquad n_e^2 = \frac{\varepsilon_p\varepsilon_g}{\boldsymbol{n}\varepsilon\boldsymbol{n}}. \tag{11}$$

Here, $\boldsymbol{p}_o$ and $\boldsymbol{p}_e$ are vectors of ray refraction [35]. If multiplied by c (light velocity in vacuum), they equal in magnitude to a ray velocity directed along the wave energy propagation. Note, that $n_o\boldsymbol{n}\boldsymbol{p}_o=n_e\boldsymbol{n}\boldsymbol{p}_e=1$, which means synchronism of a phase and energy propagation.

Substituting the direction $\boldsymbol{c}_1$ of the cone (Eq. (6)) generator into Eq. (11), we find that the ordinary ray is directed along the biradial. The extraordinary ray is directed along the vector

$$\boldsymbol{g}_R = \varepsilon\boldsymbol{c}_1 = \varepsilon k_p\boldsymbol{u}_p + \varepsilon k_g\boldsymbol{u}_g. \tag{12}$$

For the second cone generator $\boldsymbol{g}_N$, on the contrary, the ordinary ray being parallel to $\boldsymbol{g}_N$, does not coincide with the direction of the biradial $\boldsymbol{c}_1$, but the extraordinary ray is directed along it. Three vectors $\boldsymbol{c}_1$, $\boldsymbol{g}_N$ and $\boldsymbol{g}_R$, in essence, define the cross-sections of the ray cone and the cone of external conical refraction (the cone of wave normals) by the principal optical indicatrix plane N_p-N_g. The directions of these vectors can be properly specified in this plane by corresponding angles. To define these angles with respect to the N_p axis of the optical indicatrix, see Fig. 1(b), is convenient because in many crystals this axis coincides with the crystallographic axis b:

$$\tan\beta_{bir} = \frac{\mathbf{c}_1\mathbf{u}_g}{\mathbf{c}_1\mathbf{u}_p} = \frac{k_g}{k_p}, \tag{13a}$$

$$\tan\beta_N = \frac{\mathbf{g}_N\mathbf{u}_g}{\mathbf{g}_N\mathbf{u}_p} = \frac{\varepsilon_p}{\varepsilon_g}\tan\beta_{bir} = \frac{\varepsilon_p\sqrt{(\varepsilon_3-\varepsilon_m)}}{\varepsilon_g\sqrt{(\varepsilon_m-\varepsilon_p)}}, \tag{13b}$$

$$\tan\beta_R = \frac{\mathbf{g}_R\mathbf{u}_g}{\mathbf{g}_R\mathbf{u}_p} = \frac{\varepsilon_g}{\varepsilon_p}\tan\beta_{bir} = \frac{\varepsilon_g\sqrt{(\varepsilon_g-\varepsilon_m)}}{\varepsilon_p\sqrt{(\varepsilon_m-\varepsilon_p)}}. \tag{13c}$$

As $\varepsilon_p<\varepsilon_g$ by definition, so $\beta_R>\beta_{bir}>\beta_N$. If knowing these angles, we can always find the apex angle of the cone of normal, $\chi_N=\beta_{bri}-\beta_N$, and the apex angle of the ray cone, $\chi_R\beta_R-\beta_{bir}$, in the N_p-N_g plane (perpendicular to the ort $\boldsymbol{u}_m$).

In general, two isonormal waves propagating in any direction of the phase normal $\boldsymbol{n}$ have refractive indices depending of its orientation relatively the binormals $\boldsymbol{c'}_1$ and $\boldsymbol{c'}_2$ [35]:

$$\frac{1}{n_\pm^2} = \frac{1}{\varepsilon_m} + \frac{1}{2}\left(\frac{1}{\varepsilon_p}-\frac{1}{\varepsilon_g}\right)([\boldsymbol{nc}_1'][\boldsymbol{nc}_2'] \pm \sqrt{[\boldsymbol{nc}_1']^2[\boldsymbol{nc}_2']^2}) \tag{14}$$

Here, the square brackets mean the vector product of the two vectors; the scalar product of two vectors $[\boldsymbol{nc'}_1]$ and $[\boldsymbol{nc'}_2]$ and their squares can be written in the form:

$$[\boldsymbol{nc}_1'][\boldsymbol{nc}_2'] = \boldsymbol{c}_1'\boldsymbol{c}_2' - (\boldsymbol{nc}_1')(\boldsymbol{nc}_2'), \tag{15a}$$

$$[\boldsymbol{nc}_{1,2}']^2 = 1-(\boldsymbol{nc}_{1,2}')^2. \tag{15b}$$

The corresponding vectors of the ray refraction are given by [35]

$$\boldsymbol{p}_\pm = n_\pm\frac{n_\pm^2(\boldsymbol{n}\varepsilon\boldsymbol{n}\cdot\boldsymbol{n}+\varepsilon\boldsymbol{n}) - (\overline{\varepsilon_I}-\overline{\varepsilon})\boldsymbol{n}}{n_\pm^2\boldsymbol{n}\varepsilon\boldsymbol{n} - \det(\varepsilon)}. \tag{16}$$

Here, $\overline{\varepsilon}$ means a tensor mutual with ε, $\overline{\varepsilon_I}$ is its trace: $\overline{\varepsilon}=\varepsilon\varepsilon^{-1}$, $\overline{\varepsilon_I}=\varepsilon_m\varepsilon_g+\varepsilon_p\varepsilon_g+\varepsilon_p\varepsilon_m$, $det\,(\varepsilon)=\varepsilon_p\varepsilon_m\varepsilon_g$. In Eq. (16), the scalar denominator may be omitted, because it does affect the determination of the directions of $\boldsymbol{p}_\pm$, except of its sign which is negative in some cases. One of the waves with the subscript "–" for all directions of the cone of normals, Eq. (6), hasthe ray refraction vector directed along $\boldsymbol{c}_1$. The ray refraction vectors of the second wave with the subscript "+" form a cone of rays. In order to find this cone, it is necessary to determine the wave normals which define the ray refraction vectors, Eq. (16), and satisfy Eqs. (6) and (7). Forthis, we introduce an angle α in the plane of cross-section defined by Eq. (9), as shown in Fig. 1(b). Then the radius-vector $\boldsymbol{r'}$ of the circle can be written as $\boldsymbol{r'}=2Rcos^2\alpha\,\boldsymbol{d}+Rsin(2\alpha)\,\boldsymbol{u}_m$ so for every cone generator $l\boldsymbol{c}_1+\boldsymbol{r'}$, the corresponding wave normal after normalization can be written as:

$$\boldsymbol{n} = \frac{\boldsymbol{c}_1 + \pi(2cos^2\alpha\boldsymbol{d} + sin2\alpha\boldsymbol{u}_m)\tan(\chi_N/2)}{\sqrt{1+(\tan\chi_N\cos\alpha)^2}}. \tag{17}$$

Due to the symmetry reasons, the angle α can be restricted to the region $0\le\alpha\le\pi/2$. Eqs. (14), (16) and (17) are rather complex, so it is difficult to deduce from them the ray cone equation in an analytical form. Thus, mostly a numerical analysis will be used hereinafter. Four biaxial crystals of different anisotropy were chosen for calculations, potassium gadolinium tungstate (KGW), $(NH_4)_2C_2O_4\,H_2O$ (ammonium oxalate), and L-N-(5-Nitro-2-peridyl)leucinol (NPLO). The first one when doped with trivalent rare-earth ions is a well-known laser crystal, while the next two are organic crystals having large (particularly NPLO) optical anisotropy.

The experiments in [25,26] were carried out with ortorhombic sulfur crystals, therefore it was included into our consideration too. Sulfur posses a large birefringence but poor heat conductivity which makes it brittle and unsuitable for practical applications. The principal refractive indices of these crystals are listed in Table 1.

3. Discussion

Let us find the curve in the cross-section of the ray cone by the same plane as in the case of the cone of normals. To do this, we determine three projections of $\boldsymbol{p}_+$(we remind here that $\boldsymbol{p}_-\|\boldsymbol{c}_1$) on $\boldsymbol{c}_1$, $\boldsymbol{u}_m$ and $\boldsymbol{d}$

Table 1
Principal refractive indices of the crystals used in calculations.

Crystal	λ, nm	Principal refractive indices			Point group	Ref.
		n_p	n_m	n_g		
KGW	632.8	2.01348	2.04580	2.08608	C2/c	[37]
AO[a]	667.8	1.4362	1.5426	1.5892	222[b]	[38]
NPLO	632.8	1.4570	1.6310	1.9330	222	[38]
Sulfur	508.0	1.9876	2.0938	2.3380	2/m2/m2/m[c]	[39]

[a] Ammonium oxalate (AO).
[b] Orthorhombic α-modification.
[c] Optically positive crystal (all others are negative).

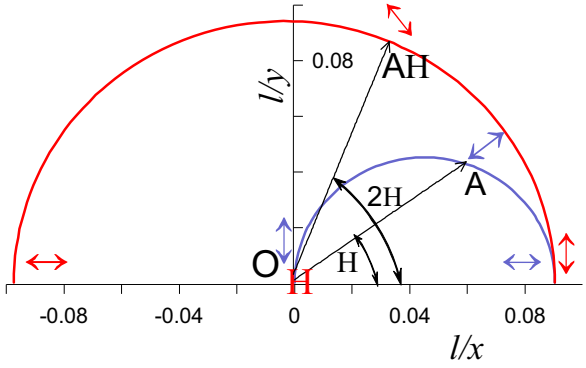

Fig. 2. Cross-section by plane orthogonal to the biradial $\boldsymbol{c}_1$ of the cone of normals (small semicircle) and the cone of rays (large semicircle) for ammonium oxalate. O is the location of the biradial, the two-sided arrows show the polarization of the vector $\boldsymbol{D}$ (see the text for the details).

orts and normalize them so that the condition $\boldsymbol{p}_+\boldsymbol{c}_1=1$ is fulfilled. When α takes all values in the interval [0, π/2], the generator of the cone of normals circumscribes a semicircle in the cross section plane while the generator of the ray cone circumscribes a curve close to a semicircle, see Fig. 2. The ratio of the curve diameters in $\boldsymbol{d}$ and $\boldsymbol{u}_m$ directions is close to unity (0.9996, 0.9956 and 0.9654 for KGW, ammonium oxalate and NPLO, respectively). A large difference in the diameters of the cross-sections of the ray cone and the cone of normals is clearly seen from Fig. 1 and Fig. 2; their ratio is close to 2 (1.9918, 2.0774 and 1.83 for KGW, ammonium oxalate and NPLO, respectively). This is true for all biaxial crystals. Indeed, as it follows from Eq. (13), the ratio of $tan(\beta_R - \beta_{bir})$ to $tan(\chi_N)$ ranges between $\varepsilon_p/\varepsilon_g$ and $\varepsilon_g/\varepsilon_p$ (that is near 1). This means that the apex angle of the ray cone is nearly twice as large as that of the cone of normals and the biradial $\boldsymbol{c}_1$ is close to the position of a bisector of the ray cone apex angle.

Calculations presented in Table 2 prove these conclusions. At $\alpha=\pi/4$, the radius-vector $\boldsymbol{r}'$ of the circle cross section of the cone of normals is parallel to $\boldsymbol{u}_m$. Simultaneously, the corresponding radius-vector of the cross section curve of the ray cone reaches the same direction that is a result of its angular speed which is on average twice as large as that for radius-vector $\boldsymbol{r}'$. The size (diameter) of the ray cone cross-section in this direction (transversal diameter) is slightly larger than that in the cross section by the N_p-N_g principal plane. Thus, the apex angle in this cross section passing through the vertex of the cone and this transversal diameter, which we denote in Table 2 as χ_S, is slightly differ from χ_R. For NPLO with its huge optical anisotropy, the largest value of the transversal diameter deviates from the direction of $\boldsymbol{u}_m$ and is observed at α=44° (136° if we include into the consideration of α a wider angular interval; the angle χ_S in Table 2 is given for this diameter). This means that only the inverse center exists as a symmetry element of the ray cross section curve but it is noticeable only in crystals with exclusive optical anisotropy. Mirror symmetry of the ray cross section curve relatively to the N_p-N_g principal plane can be regarded, strictly speaking, only approximately. Nevertheless, even for such a strongly birefringent crystal as ammonium oxalate, the deviation from the mirror symmetry is negligibly small. The ratio of the tangent of the apex angle of the ECR cone χ_N to that of ICR cone is equal to $n_p n_g/n_m^2$. Because this ratio is close to unity, the apex angles of both cones are close to each other. In KGW, for example, these angles are 2°13′ and 2°08′ for ECR and ICR cones respectively.

The polarization distribution of the vector of electrical induction $\boldsymbol{D}$ within the cross section curves is illustrated in Fig. 2 by two-sided arrows. For any point A of the circle cross section of the wave normal cone specified by an angle α, the vector $\boldsymbol{D}_-$ located in the plane containing a wave normal $\boldsymbol{n}$ and the ray refraction vector $\boldsymbol{p}_-\|\boldsymbol{c}_1$ is parallel to the line OA ($\boldsymbol{D}_-\|[\boldsymbol{np}_-]$). In the N_p-N_g principal plane at α=0 and α=π/2, it is the polarization of the extraordinary or ordinary waves, respectively. For the second wave with the vector $\boldsymbol{D}_+$ being orthogonal to $\boldsymbol{D}_-$, the corresponding point A′ is determined approximately by the angle 2α (the angular speed of movement along the circle for any point A on the average is half of that for the corresponding point A′ of the cross section of the cone of rays).

The cone of ECR is caused by the cone of waves incident on a crystal from an external medium. This cone is easily found using the Snell's law; it splits into two cones due to the two isonomal waves in a crystal:

$$\chi_\pm = \arcsin(n_\pm \sin(\hat{n, c_1})), \tag{18}$$

where air is supposed to be an ambient medium. In Eq. (18), $\boldsymbol{n}$ belongs to the cone of wave nomals, Eq. (6), and depends on the angle α which defines the position of the plane of incidence relatively to the N_p-N_g principal plane of the optical indicatrix (hereafter, the principal plane of incidence). As is clear from the calculations carried out for the crystal cut orthogonal to the biradial, the cross-section curves of incident wave cones in the plane parallel to the crystal facet are close to circles (even for ammonium oxalate, the ratio of mutually orthogonal diameters is 0.998). For the direction of an incident wave parallel to the biradial, the cones, Eq. (18), are in contact and $\chi_+ - \chi_- = 0$. The maximum difference between χ_+ and χ_- is observed in the principal plane of incidence when the refracted waves propagate along $\boldsymbol{g}_N$. In this case, the difference reaches 2′ for ammonium oxalate and only 0.3′ for KGW and thus can be neglected for these and practically for all other crystals (but for NPLO it has a noticeable value equal to 1°09′). Such a small difference is stipulated by the proximity of $\boldsymbol{g}_N$ to the direction of the crystal binormal $\boldsymbol{c}'_1$ when n_+ and n_- are equal (for example, in KGW the angle between $\boldsymbol{g}_N$ and $\boldsymbol{c}'_1$ is ~4°). Calculated values of the apex angles for cones, Eq. (18), are presented in Table 3.

Table 2
Angles between $\boldsymbol{u}_p$ (the direction of the N_p axis of the optical indicatrix) and the biradial (β_{bir}), $\boldsymbol{u}_p$ and the ray cone generators (β_R, β_N), apex angles of the cone of wave normals (χ_N), the ray cone in the principal N_p-N_g plane of the optical indicatrix (χ_R) and in the plane orthogonal to it (χ_S).

Crystal	β_{bir}	β_R	β_N	χ_N	χ_R	χ_S
KGW	48°24′	50°24′	46°23′	2°13′	4°02′	4°02′
AO	34°10′	39°43′	28°60′	5°98′	10°47′	10°47′
NPLO	54°45′	68°77′	38°48′	15°57′	29°20′	30°20′
Sulfur	57°40′	65°25′	48°44′	8°53′	16°38′	16°37′

Table 3
The apex angles for the cones of incident waves for the considered crystals.

Crystal	Apex angle	
	χ_+	χ_-
KGW	4°08′	4°09′
Ammonium Oxalate	7°59′	8°01′
NPLO	26°38′	27°47′
Sulfur	18°51′	19°06′

The cone of incident waves χ_+ is related to the ray cone inside a crystal. It should be noted that the ray cone being a result of birefringence always arises inside the crystal even if the incident convergent beam does not contain waves making the cone χ_+. The second cone of the incident waves χ_- produces inside the crystal refracted waves for which the rays are parallel to $\boldsymbol{c}_1$. In the principal plane of incidence, the wave normal of one of these refracted waves is directed along $\boldsymbol{c}_1$ (zero angle of refraction). The second wave is an ordinary wave; for this wave the angle of refraction is equal to the apex angle of the cone of normals χ_N and the refractive index $n_-=n_m$. Hence, neglecting the difference between χ_- and χ_+ and taking into account Eq. (18), we find the apex angle of the cone of incident waves $\chi_{inc}=\chi_-$ as:

$$\chi_{inc} = \arccos(n_m(\sin\chi_N)) = \arcsin\left(n_m\sqrt{\frac{(\varepsilon_m-\varepsilon_p)(\varepsilon_g-\varepsilon_m)}{\varepsilon_p\varepsilon_m+\varepsilon_g(\varepsilon_m-\varepsilon_p)}}\right). \quad (19)$$

A hollow cone of incident convergent beam is rearranged within the crystal into a single ray of light propagating along the biradial and into a cone of rays with its axis close to the direction of the biradial. The refraction at the exit facet of a plane-parallel crystal plate leads to the appearance of two cones and two light rings at a screen behind the plate. Axes of the cones are not parallel but their directions differ slightly and therefore the cones and the rings for crystals with a small and moderate optical anisotropy are practically coaxial. A special polarization distribution takes place for each of the cones. In Fig. 3(a), the orientation of the electric vector $\boldsymbol{E}$ of the wave field is shown by two-sided arrows (located in the plane of incidence) or by dot (if $\boldsymbol{E}$ is perpendicular to the plane). A full picture of the polarization distribution for both light rings at the screen is presented in Fig. 3(b). For the two light rings, the polarization planes are mutually perpendicular at the points lying on one radius. It is provided by double angular speed of movement with the change of α angle for points at the ray cone inside the crystal, as mentioned above. For the inner circle, as shown in Fig. 2 and Fig. 3(b), the orientation of an electric vector $\boldsymbol{E}$ ($\boldsymbol{D}$ within a crystal) is in line with that in the case of ICR.

According to Fig. 2 and Fig. 3, over the circumference of the outer (ray) ring, the vector $\boldsymbol{E}$ changes from the direction in plane for the left ray in the principal plane of incidence to the direction perpendicular to this plane for the right ray and vice versa for the inner cone. These peculiarities of the polarization distribution over the rings were noted by Mikhailychenko in his observations of ECR in the sulfur crystal plate [25,26]. He has also found that the angle of ECR for sulfur is ~7° [25] and it is almost 2-times increased after crossing the crystal-air surface. As it follows from our calculations, the angle of ECR is about 9° for this situation (see χ_N in Table 2). After leaving the exit face, light spreads into a cone with more than doubled apex angle (the angle χ_- in Table 3). Such a difference seems to be related to the accuracy of measured refractive indices (for a more detailed discussion, see the next section). As noted in [25], the spacing between the rings of ECR is determined by the crystal thickness h. In experiments with sulfur [25], the crystal thickness was 12 mm and the measured spacing x was 2 mm. From Fig. 3, it is easy to deduce that the spacing is not a constant and changes between $x_1=h\ tan(\chi_N)$ and $x_2=h\ tan(\chi_R-\chi_N)$ or 1.6 and 1.9 mm (while for χ_N~7° [25] the spacing is less than 1.5 mm). It should be emphasized that the spacing is also strongly dependent on the crystal anisotropy and, for instance, for KGW of the same thickness it equals to only 0.5 mm.

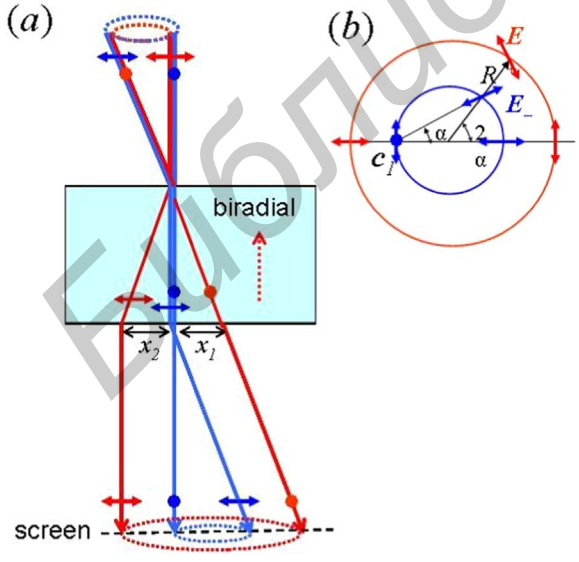

Fig. 3. External conical refraction. (a) Cones of incident waves giving rise to the ray filament and the cone of rays inside a crystal and two light cones behind the crystal plate; x_1 and x_2 are the spacings between the light rings. (b) Two light rings at a screen behind the crystal plate. Polarization of the electric vector $\boldsymbol{E}$ is shown by two-sided arrows. For inner ($\boldsymbol{E}_-$) and outer ($\boldsymbol{E}_+$) rings, they are mutually perpendicular at points lying on one radius.

4. Dispersion of the ECR characteristic angles

High light intensity within the crystal in the direction of its biradials owing to the beam filamentation can be achieved easily in the case of ECR that is interesting for nonlinear applications of the phenomenon. A promising crystal family for nonlinear and laser applications is MDTs. MDTs possess relatively high optical anisotropy and they can be grown of large sizes, high quality and homogeneity. Three crystals of the family, namely $KGd(WO_4)_2$ (KGW), $KLu(WO_4)_2$ (KLuW) and $KY(WO_4)_2$ (KYW) were chosen for calculations. Dispersion of their principal refractive indices can be found in the literature [37,40–43]. The Sellmeier equation was used by different authors to model the dispersion of the principal refractive indices n_j or the principal dielectric impermeabilities $\varepsilon_i=n_i^2$, (j= p, m, g), the last is more physically justified.

It should be pointed out that, as is seen from Eqs. (3) and (13), the directions of the optical axes (binomals and biradials) and also the vectors $\boldsymbol{g}_N$, $\boldsymbol{g}_R$ depend on differences of the principal dielectric impermeabilities which are proportional to the principal refractive indices. Hence it follows that even a slight change of one of the three principal refractive indices makes a marked deference in the orientations of these directions. Such an extreme sensitivity on the refractive index differences was noted in [44] for the angle of the cone of ICR and in [45] for the binormal orientation. In the latter paper, the authors have found parameters of the three-term Sellmeier dispersion formula for Ho^{3+}:KYW [46] and they corrected the fitting parameters for the refractive index n_g of KGW [40] (pure and doped with Nd^{3+} ions) using an original approach for the determination of the optical axis dispersion based on ICR. These parameters give very precisely the shape of the dispersion curves for specific directions in the crystal (in our case, the angles β_{bir}, β_R and β_N), although their absolute values may differ remarkably (± 1° for the directions of binormals [45,46]). In monoclinic crystals, only one of the axes of the orthonormal dielectric frame $\{N_p, N_m, N_g\}$, namely the N_p axis, coincides with the crystallographic axis ($\boldsymbol{b}$-axis). Other two axes N_m, N_g (and two crystallographic axes $\boldsymbol{a}$and $\boldsymbol{c}$) are located in the plane perpendicular to the $\boldsymbol{b}$-axis and their position is wavelength-dependent [47]. Only taking into account this peculiarity of the monoclinic crystals, the dispersion of their principal refractive indices can be determined correctly. This was done in [48] where the behavior of the dielectric frame as a function of wavelength was measured for the first time for three MDTs KGW, KYW and the Sellmeier equations of the principal refractive indices were refined in the spectral range of 0.4–1.6 μm. These data were used in our calculations.

Fig. 4 illustrates the dispersion of the biradial orientation in the three MDTs. For comparison, the dispersion curves for the binormal

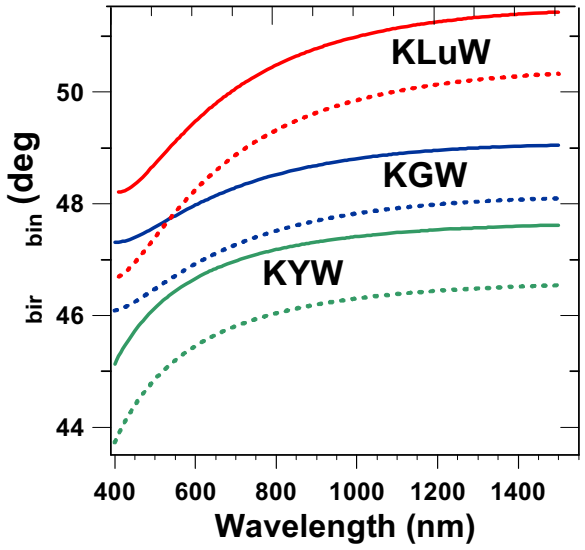

Fig. 4. Dispersion curves of the angle between the biradial (*solid* lines), binormal (*dashed* lines) and the N_p axis for MDTs.

orientation defined by the angle β_{bin}, where

$$tg\beta_{bin}=\frac{n_p}{n_g}tg\beta_{bir} \quad , \tag{20}$$

are shown in too. From Eq. (20), it is obvious that in all crystals $\beta_{bin} < \beta_{bir}$. Notice that our crystals the dispersion behavior of both angles β_{bin} and β_{bir} is almost identical.

The dispersion of the apex angles of ECR χ_N and the ray cone χ_R is presented in Fig. 5. It is evident from this figure that the shapes of the dispersion curves for χ_N and χ_R are fully identical and differ only by a slightly more strong dependence χ_R on the wavelength. If comparing the dispersion curve for the cone of incident waves (Fig. 6) with that of the rays inside the crystal χ_R, one can see that they match almost exactly. In fact, as it was shown above, the apex angle χ_R is equal roughly to $2\chi_N$. It also follows from Eq. (19) that at small χ_N, we can approximate $\chi_{inc}\approx n_m\chi_N$. For MDTs, $n_m\sim 2$ so that $\chi_R\approx\chi_{inc}$. As it is clear from Tables 2, 3, for KGW at the wavelength of 632.8 nm χ_R=4°02′ while χ_{inc}=χ_-=4°09′ so the difference between them is only 7′. In KGW, KYW and KLuW, the difference $\chi_{inc}-\chi_R$ is less than 20′,

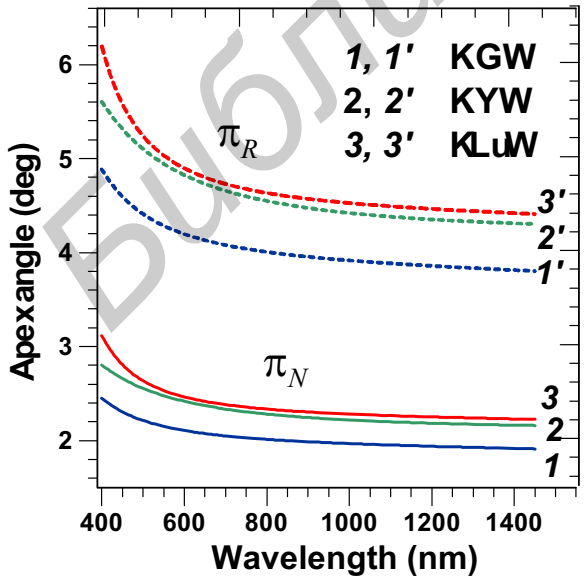

Fig. 5. Dispersion of the angle of ECR χ_N (*solid* lines) and the apex angle of the ray cone χ_R (*dashed* lines) for MDTs.

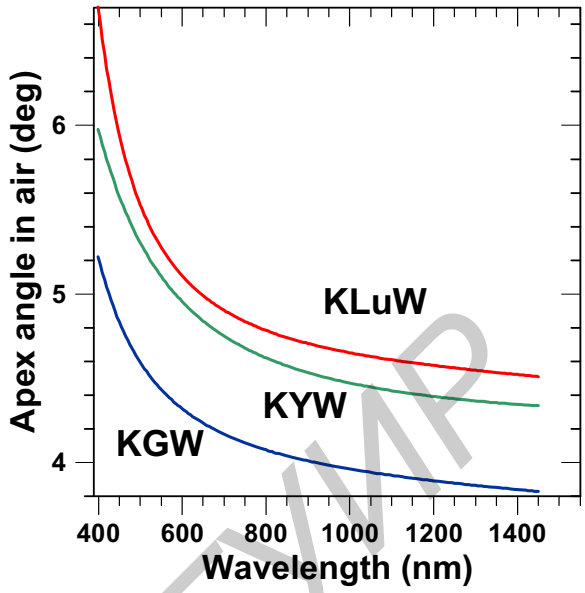

Fig. 6. Dispersion of the apex angle of the cone of incident waves χ_{inc} for MDTs, according to Eq. (19).

22′ and 31′, respectively (maximum values observed at 400 nm) for the whole studied spectral range. Thus, the ray cone in the MDT crystals approximately coincides with the cone of incident waves. Hence it follows that the cone of refracted waves at the crystal plate exit face nearly is a continuation of the ray cone inside the crystal.

5. Conclusions

The hollow cone of ECR is a cone of wave normals inside a crystal. This cone is related to two sets of rays owing to the birefringence. One set contains the rays propagating along the crystal biradial, and the second one forms a cone of rays. Its cross section by a plane orthogonal to the biradial is close to a circle. This is also true for the hollow cone of the waves incident on the crystal which give rise to the cone of ECR. The apex angle of the ray cone is nearly twice as large as that of the cone of normals so that its axis is close to the direction of the biradial. Two sets of rays belong to two sets of isonomal waves in a crystal. Every pair of isonomal waves have different refractive indices and so through the Snell's law should be related with two different cones of incident waves. Because directions of the biradial and binormal (usually referred as an optical axes for direction of which the refractive indices of both waves in the crystals are equal) are close, the difference in the value of these refractive indices is small therefore the difference for the cones of incident waves is insignificant and practically in all cases can be ignored. After leaving the exit face of a plane-parallel crystal plate, the light rays that propagate along the biradial spread into a cone again (the first cone). The cone of rays within the plate after refracting at its exit face transforms into the second cone. Thus, two light rings are observed at a screen after the crystal plate, in accordance with [25,26]. Polarization planes for the two rings of ECR are mutually perpendicular at the points lying on the same radius. For the inner ring, the polarization distribution is the same as in the case of ICR [24]. Keeping in mind the possibility of energy concentration along the biradial, we should form the corresponding polarization distribution in the hollow cone of the incident waves to circumvent an appearance of the ray cone inside and the second cone behind the crystal. This can be achieved using ICR to form a hollow cone of rays with the needed polarization distribution in air and then focusing it on a surface of another crystal surface. It was just this scheme which was recently realized in [31].

Acknowledgment

This research did not receive any specific grant from funding agencies in the public, commercial, or not-for-profit sectors. The author is indebted to Dr. Pavel Loiko for his valuable comments and manuscript revision.

References

[1] J.G. O'Hara, The prediction and discovery of conical refraction by William Rowan Hamilton and Humphrey Lloyd (1832–1833), Proc. R. Ir. Acad. 82A (1982) 231–257.
[2] M.V. Berry, M.R. Jeffrey, Conical diffraction: Hamilton's diabolical point at the heart of crystal optics, Prog. Opt. 50 (2007) 13–50.
[3] W. Voigt, Theoretisches und experimentalles zur aufklaerung des optischen verhaltens aktiver kristalle, Ann. Phys. 18 (1905) 645–694.
[4] A.J. Schell, N. Bloembergen, Laser studies of internal conical diffraction. I. Quantitative comparison of experimental and theoretical conical intensity distribution in aragonite, J. Opt. Soc. Am. 68 (1978) 1093–1098.
[5] V.V. Filippov, Energy flux of homogeneous waves under conical refraction and induced gyrotropy, Opt. Spectrosc. 42 (1977) 553–556.
[6] E. Lalor, An analytical approach to the theory of internal conical refraction, J. Math. Phys. 13 (1972) 449–454.
[7] A.M. Belsky, M.A. Stepanov, Internal conical refraction of coherent light beams, Opt. Commun. 167 (1999) 1–5.
[8] A.M. Belsky, M.A. Stepanov, Internal conical refraction of Bessel light beams, Opt. Spectrosc. 92 (2002) 455–458.
[9] R.T. Darcy, D. McCloskey, K.E. Ballantine, J.G. Lunney, P.R. Eastham, J.F. Donegan, Conical diffraction intensity profiles generated using a top-hat input beam, Opt. Express 22 (2014) 11290–11300.
[10] M.V. Berry, M.R. Jeffrey, J.G. Lunney, Conical diffraction: observations and theory, Proc. R. Soc. A 462 (2007) 1629–1642.
[11] A. Abdolvand, K.G. Wilcox, T.K. Kalkandjiev, E.U. Rafailov, Conical refraction Nd:KGd(WO_4)$_2$ laser, Opt. Express 18 (2010) 2735–2759.
[12] K.G. Wilcox, A. Abdolvand, T.K. Kalkandjiev, E.U. Rafailov, Laser with simultaneous Gaussian and conical refraction outputs, Appl. Phys. B99 (2010) 619–622.
[13] C. McDonald, C. McDougall, E. Rafailov, D. McGloin, Characterising conical refraction optical tweezers, Opt. Lett. 39 (2014) 6691–6694.
[14] V. Peet, Biaxial crystal as a versatile mode converter, J. Opt. 12 (2010) 095706.
[15] G.S. Sokolovskii, D.J. Carnegie, T.K. Kalkandjiev, E.U. Rafailov, Conical refraction: new observations and a dual cone model, Opt. Express 21 (2013) 11125–11131.
[16] S.D. Grant, A. Abdolvand, Evolution of conically diffracted Gaussian beams in free space, Opt. Express 22 (2014) 3880–3886.
[17] A.J. Schell, N. Bloembergen, Laser studies of internal conical diffraction. II. Intensity patterns in an optically active crystal, α-iodic acid, J. Opt. Soc. Am. 68 (1978) 1098–1106.
[18] A.M. Belsky, M.A. Stepanov, Internal conical refraction of light beams in biaxial gyrotropic crystals, Opt. Commun. 204 (2002) 1–6.
[19] H. Shih, N. Bloembergen, Conical refraction in second-harmonic generation, Phys. Rev. 184 (1969) 895–904.
[20] R.A. Indik, A.C. Newell, Conical refraction and nonlinearity, Opt. Express 14 (2006) 10614–10620.
[21] A. Turpin, Y.V. Loiko, T.K. Kalkandjiev, J. Trull, C. Cojocaru, J. Mompart, Type I and type II second harmonic generation of conically refracted beams, Opt. Lett. 38 (2013) 2484–2486.
[22] S.D. Grant, S.A. Zolotovskaya, T.K. Kalkandjiev, W.A. Gillespie, A. Abdolvand, On the frequency-doubled conically-refracted Gaussian beam, Opt. Express 22 (2014) 21347–21353.
[23] T.S. Velichkina, O.I. Vasil'eva, A.I. Israilenko, I.A. Yakovlev, Demonstration of phenomena of conical refraction, Sov. Phys. Usp. (USA) 23 (1980) 176–177.
[24] J.P. Frve, B. Boulanger, G. Marnier, Experimental study of internal and external conical refractions in KTP, Opt. Commun. 105 (1994) 243–252.
[25] Yu. P Mikhailychenko, Large scale demonstrations on conical refraction. ⟨http://www.demophys.tsu.ru/Original/Hamilton/Hamilton.html⟩ /(accessed 11.09.16), 2005.
[26] Yu. P. Mikhailichenko, Conical refraction: experiments and large-scale demonstrations, Russ. Phys. J. 50 (2007) 778–795.
[27] Conical refraction becomes practical, Laser focus world 06/01,⟨http://www.laserfocusworld.com/articles/print/volume-40/issue-6/world-news/world-news/conical-refraction-becomes-practical.html/⟩, 2004 (accessed 11.09.16)
[28] M. Born, E. Wolf, Principles of Optics, sixth ed., chapter 14, Pergamon Press, Oxford, 1980
[29] A.M. Belsky, A.P. Khapalyuk, Propagation of confined light beams along the beam axes (axes of single ray velocity) of biaxial crystals, Opt. Spectrosc. 44 (1978) 312–315.
[30] T.K.Kalkandjiev, M.A.Bursukova, Conical refraction: an experimental introduction, in: J.T. Sheridan, F. Wyrowski, (Eds), Photon Management III, Proc. SPIE, 6994 2008, 69940B.
[31] R.Cattoor, Investigation on 2 mkm laser sources based on monoclinic crystals. Cristallography. Universite de Bordeaux, thesis⟨https://tel.archives-ouvertes.fr/tel-01249609/document/⟩, 2015 (accessed 11.09.16).
[32] L. Junhai, U. Griebner, V. Petrov, Z. Huaijin, Z. Jianxiu, W. Jiyang, Efficient continuouswave and Q-switched operation of a diode-pumped Yb:KLu(WO4)2 laser with self-Raman conversion, Opt. Lett. 30 (2005) 2427–2429.
[33] T.T. Basiev, New crystals for Raman lasers, Phys. Solid State 47 (2005) 1400–1405.
[34] J.A. Piper, H.M. Pask, Crystalline Raman lasers, IEEE J. Sel. Top. Quantum Electron. 13 (2007) 692–704.
[35] F.I.Fedorov, Optics of anisotropic media, Izd. Akad. Nauk BSSR, Minsk, (in Russian), 1957.
[36] F.I.Fedorov, V.V.Filippov, Reflection and refraction of light by transparent crystals, Nauka i Tekhnika, Minsk(in Russian), 1976.
[37] V.V. Filippov, N.V. Kuleshov, I.T. Bodnar, Negative thermo-optical coefficients and athermal directions in monoclinic KGd(WO_4)$_2$ and KY(WO_4)$_2$ laser host crystals in the visible region, Appl. Phys. B 87 (2007) 611–614.
[38] V.G. Dmitriev, G.G. Gurzadyan, D.N. Nikogosyan, Handbook of Nonlinear Optical Crystals, third revised edition, Springer, 1999.
[39] Landolt-Börnstein, Group III Condensed Matter. Vol. 41C (Non-Tetrahedrally Bonded Elements and Binary Compounds I), SpringerVerlag, Berlin Heidelberg, 1998.
[40] M. Pujol, M. Rico, C. Zaldo, R. Solé, V. Nikolov, X. Solans, M. Aguiló, F. Diaz, Crystalline structure and optical spectroscopy of Er^{3+}-doped KGd(WO4)2 single crystals, Appl. Phys. B 68 (1999) 187–197.
[41] A. Kaminskii, A. Konstantinova, V. Orekhova, A. Butashin, R. Klevtsova, A. Pavlyuk, Optical and nonlinear laser properties of the χ (3)-active monoclinic α-KY(WO_4)$_2$ crystals, Crystallogr. Rep. 46 (2001) 665–672.
[42] M.C. Pujol, X. Mateos, A. Aznar, X. Solans, S. Suriñach, J. Massons, F. Díaz, M. Aguiló, Structural redetermination, thermal expansion and refractive indices of KLu(WO_4)$_2$, J. Appl. Crystallogr. 39 (2006) 230–236.
[43] X. Mateos, R. Solé, Jna Gavaldà, M. Aguiló, J. Massons, F. Díaz, Crystal growth, optical and spectroscopic characterization of monoclinic KY(WO4)$_2$ co-doped with Er^{3+} and Yb^{3+}, Opt. Mater. 28 (2006) 423–431.
[44] R.T. Darcy, D. McCloskey, K.E. Ballantine, B.D. Jennings, J.G. Lunney, P.R. Eastham, J.F. Donegan, White light conical diffraction, Opt. Express 21 (2013) 20394–20403.
[45] R. Cattoor, I. Manek-Hönninger, M. Tondusson, Ph Veber, T. Kalkandjiev, D. Rytz, L. Canioni, M. Eichhorn, Wavelength dependence of the orientation of optic axes in KGW, Appl. Phys. B 116 (2014) 831–836.
[46] R. Cattoor, I. Manek-Hönninger, M. Tondusson, T. Kalkandjiev, D. Rytz, L. Canioni, M. Eichhorn, Optic axis dispersion in double tungstate crystals and laser operation at 2 μm, Proc. SPIE 8959 (2014) 89591N.
[47] C. Traum, P.L. Inácio, C. Félix, P. Segonds, A. Peña, J. Debray, B. Boulanger, Y. Petit, D. Rytz, G. Montemezzani, P. Goldner, A. Ferrier, Direct measurement of the dielectric frame rotation of monoclinic crystals as a function of the wavelength, Opt. Mater. Express 4 (2014) 57–62.
[48] P. Loiko, P. Segonds, P.L. Inácio, A. Peña, J. Debray, D. Rytz, V. Filippov, K. Yumashev, M.C. Pujol, X. Mateos, M. Aguiló, F. Díaz, M. Eichhorn, B. Boulanger, Refined orientation of the optical axes as a function of wavelength in three monoclinic double tungstate crystals KRE(WO_4)$_2$ (RE=Gd, Y or Lu), Opt. Mater. Express 6 (2016) 2984–2990.